©2025 Published in 11th International Symposium on Intelligent Technologies in Engineering and Science 16-18 May 2025 (ISITES2025 Diyarbakır - Turkey)

Kinematic and Dynamic Analysis of a 5-DOF PRRRR Welder Robot Designed for Longitudal Profiles

*Fatih ÖZEN
[1]Beşiri Organized Industrial Zone Vocational School, Batman University, 72060, Batman, TURKEY

Abstract

In this work, a welding robot manipulator with 5-DOF was designed. The robot manipulator was designed to weld profile like extruded parts with PRRRR joints. Kinematic calculations were made using Denavit-Hartenberg method. The kinematic results of the prismatic axes were plotted between - 45º and +45º for each revolute axis as well as 0-0.1 m for prismatic axis within 10 s duration. Dynamic calculations were performed by adopting Lagrange-Euler method. The force for prismatic axis and torques for revolute axes was calculated by iterative calculations. According to results, the maximum torque was produced at the θ_2 joint with the angle of -0.9 º and 5.2 s as -5.02 Nm.

Key words: Welding robot, welding manipulator, 5-DOF, Denavit-Hartenberg method

1. Introduction

Recently, industry 4.0 has already began on the shoulders of the electronics, smart algorithms and artificial intelligence systems [1–3]. The manufacturing industry was highly affected by robotic systems. Robotic systems enabled to obtain precise and consistent parts without any human labor induced errors [4–6].

New robots or manipulators were designed according to labor types [7–11]. Articulated, carestian, scara and delta type robots are amongst them. Each of them is designed for a special job type. In literature, some researchers have developed different types of robots for special jobs. Kreutz-Delgado and Seraji [12] studied articulated type of 7-DOF manipulator for universal usage. Each of the axes were designed with revolute joints. They utilized Denavid-Hartenberg (DH) method to calculate forward kinematics. They also used Jacobian matrices to reach possible solutions to inverse kinematics. Lin et al. [13] studied 5-DOF Polishing Machine. The manipulator has three translations and two rotational axes. Kinematic analysis was studied. Kane’s equation was used fır Inverse kinematics. An efficient and real-time algorithm for inverse dynamics was developed. Li and Xu [14] presented a kinematic model of a delta like robot that has 3-PRS with variable layout angle of actuators. The researchers were making use of reciprocal screw theory for the kinematic analysis. Inverse and forward kinematics with speeds was developed. Uchiyama et al. [15] studied kinematic analysis of a 5-DOF parallel-serial hybrid robot. The robot was designed with two subdivisions of parallel and serial stage. Each subdivision was investigated separately to reach a kinematic solution. Masouleh et al. [16] studied five identical limbs of the RPUR type manipulator. This robot is designed as 5-DOF that has 2 T 3R axes. They investigated the kinematic analysis of the robot. They offered two classes of simplified designs for kinematic solutions.

*Corresponding author: Address: Beşiri Organized Industrial Zone Vocational School, Batman University, 72060, Batman, TURKEY. E-mail address: fatih.ozen@batman.edu.tr

In this work, a welding robot was designed to implement high precision torch movements for profiles and extruded parts. The kinematic structure with 5-DOF was designed as PRRRR. The kinematics and dynamics were calculated, and the results were discussed.

2. Design of the Weld Robot

The welding robot was designed to address the application of the weld to the long profiles or extruded parts. For this reason, the first axis was designed as a linear prismatic axis to easily access every longitudinal distance. The rest of the axes were designed as revolute joints. An axis was designed to execute lateral angles along longitudinal directions.

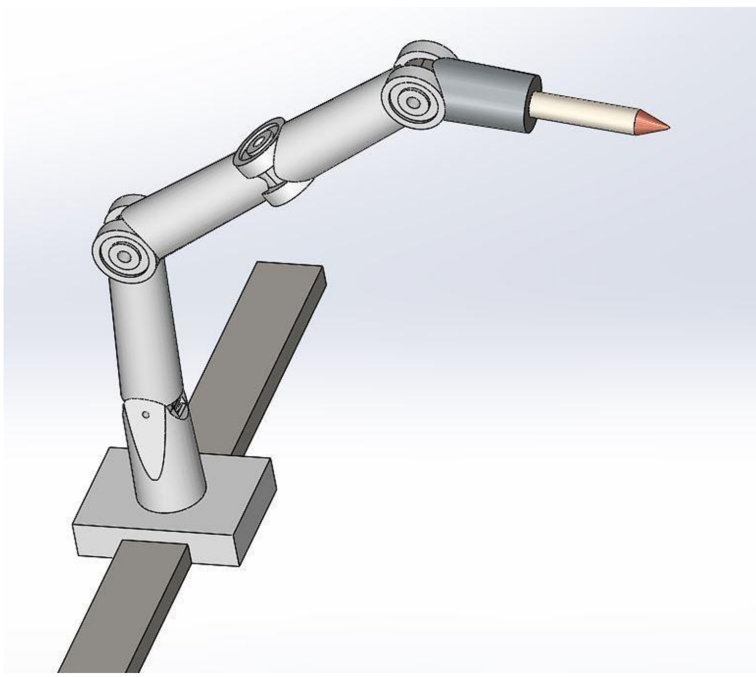

Figure 1. 3D design of the RPPPP welding robot.

The axis of rotation on the last arm is parallel to the rail axis in order to make zig-zag movements easy in the area to be welded. There are 3 axes parallel to the rail axis and 1 perpendicular to the rail axis. Such a design was chosen to enable the 3 axes to work in tight spaces, even if they are on the same axis. However, this situation brings uncertainty for the 3 axes in the inverse kinematics solution.

3. Kinematic Model and Analysis

3.1. Kinematic model

Denavit-Hartenberg (DH) method was used for kinematic calculations and analyses. Figure 2(a) shows the dimensional parameters used for the D-H table and Figure 2.b illustrates D-H notations for each axis. For the DH notations, "Z" axis implies the joint movement direction. Namely, the rotational axis is the "Z" axis for revolute joints. The rail movement direction is the "Z" axis for the prismatic joints. The direction of each arm signifies the "Y" axis. The other rest axis, "Y", mounted on the last missing axis.

Table 1 shows the D-H parameters for the kinematic calculations. Each axis length is assigned as 0.1 m. Joint angle, the joint angle θ is the controlling axis for each joint angle. It is numbered in view of the joint number. The movement limits are adjusted from 0 to 0.1 m for prismatic joints and from - $\pi/4$ to $\pi/4$ for the analysis of the position, velocity and forces. There is a twist angle of $\pi/2$ at the joint number of 3 and 4.

Table 1. D-H parameters used for kinematic calculations

Joint no.	**Joint type**	**Joint offset-b** *(m)*	**Joint angle-θ)** *(rad)*	**Link length-a** *(m)*	**Twist angle-α** *(rad)*
1	Prismatic	***Variable***	0	0.5	0
2	Revolute	0	***Variable*** (θ_2)	0.1	0
3	Revolute	0	***Variable*** (θ_3)	0.1	$\pi/2$
4	Revolute	0	***Variable*** (θ_4)	0.1	$\pi/2$
5	Revolute	0	***Variable*** (θ_5)	0.1	0

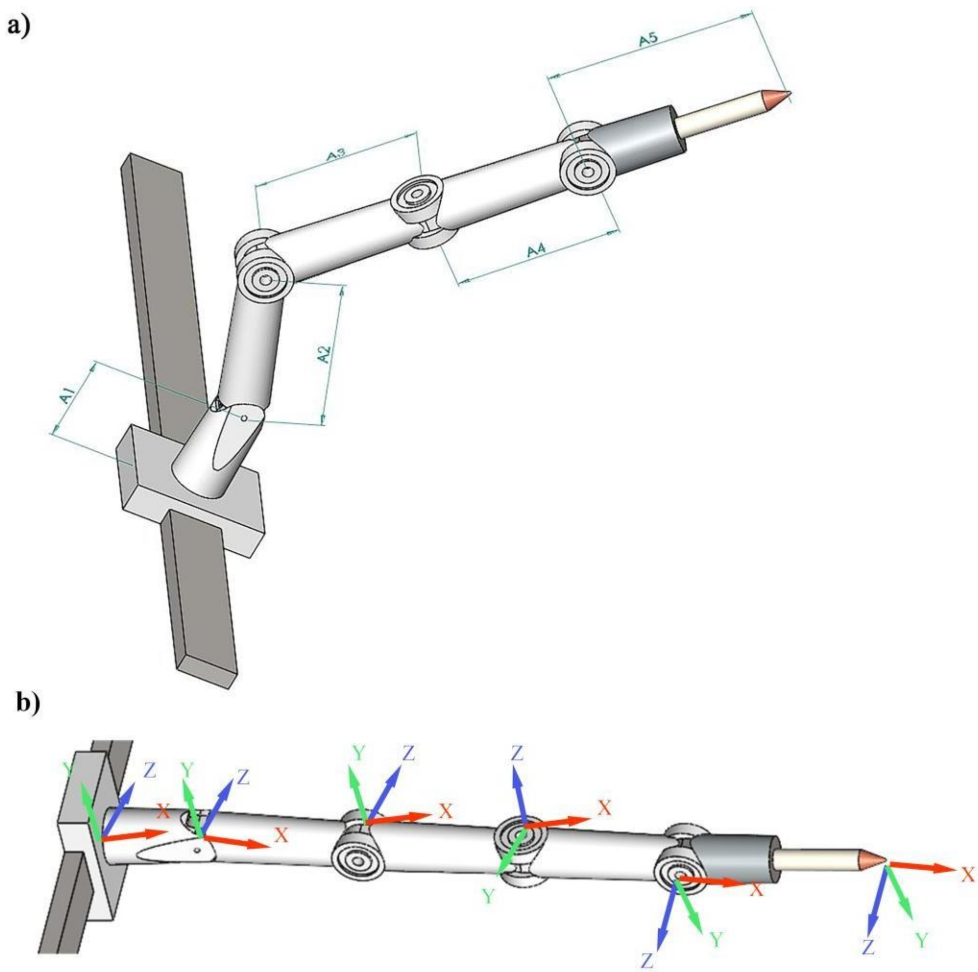

Figure 2. (a) Dimensions and **(b)** D-H notations and of the welding robot

For the calculation of the DH matrix, four different matrices should be multiplied. The rotational matrix for the joint angle is (1), translation matrix for the joint offsets is (2), translation matrix for the link offsets is (3) and rotational matrix for the twist angle is (4).

$$R_{z,\theta i} = \begin{bmatrix} cos\theta_i & -sin\theta_i & 0 & 0 \\ sin\theta_i & cos\theta_i & 0 & 0 \\ 0 & 0 & 1 & 0 \\ 0 & 0 & 0 & 1 \end{bmatrix} \tag{1}$$

$$Trans_{z,di} = \begin{bmatrix} 1 & 0 & 0 & 0 \\ 0 & 1 & 0 & 0 \\ 0 & 0 & 1 & d_i \\ 0 & 0 & 0 & 1 \end{bmatrix} \tag{2}$$

$$Trans_{x,ai} = \begin{bmatrix} 1 & 0 & 0 & a_i \\ 0 & 1 & 0 & 0 \\ 0 & 0 & 1 & 0 \\ 0 & 0 & 0 & 1 \end{bmatrix} \quad (3)$$

$$R_{z,\alpha i} = \begin{bmatrix} 1 & 0 & 0 & 0 \\ 0 & cos\alpha_i & -sin\alpha_i & 0 \\ 0 & sin\alpha_i & cos\alpha_i & 0 \\ 0 & 0 & 0 & 1 \end{bmatrix} \quad (4)$$

$$T_i^{i-1} = R_{z,\theta i} .Trans_{z,di} .Trans_{x,ai} .R_{x,\alpha i} \quad (5)$$

If (1), (2), (3) and (4) is multiplied that also described at the (5), the D-H matrix (6) is obtained. If this matrix is calculated for each link and multiplied sequentially, the T_0^5 that illustrated at (7) was obtained. This matrix multiplied matrix at (8) is composed of rotational matrix (R) and position matrix (T). R and T signifies rotational angle and poisition of the end effector, respectively.

$$T_i^{i-1} = \begin{bmatrix} cos\theta_i & -sin\theta_i cos\alpha_i & sin\theta_i sin\alpha_i & a_i cos\theta_i \\ sin\theta_i & cos\theta_i cos\alpha_i & -cos\theta_i sin\alpha_i & a_i sin\theta_i \\ 0 & sin\alpha_i & cos\alpha_i & d_i \\ 0 & 0 & 0 & 1 \end{bmatrix} \quad (6)$$

$$T_0^5 = T_0^1 T_1^2 T_2^3 T_3^4 T_4^5 \quad (7)$$

$$A = \begin{bmatrix} r_{xx} & r_{xy} & r_{xz} & P_x \\ r_{yx} & r_{yy} & r_{yz} & P_y \\ r_{zx} & r_{zy} & r_{zz} & P_z \\ 0 & 0 & 0 & 1 \end{bmatrix} = \begin{bmatrix} \square & \square & \square & \square \\ \square & R & \square & T \\ \square & \square & \square & \square \\ 0 & 0 & 0 & 1 \end{bmatrix} \quad (8)$$

The solution of the rotational matrix (R) is subdivided to $r_{\_,\_}$, where solutions for r_{xx} , $r_{xy}, r_{xz}, r_{yx}, r_{yy}, r_{yz}, r_{zx}, r_{zy}, r_{zz}$ are illustrated at (10), (11), (12), (13), (14), (15), (16) and (17), respectively.

$$r_{xx} = \sin\theta_5 (\cos\theta_2 \cos\theta_3 - \sin\theta_2 \sin\theta_3) - \cos\theta_4 \cos\theta_5 (\cos\theta_2 \sin\theta_3 + \cos\theta_3 \sin\theta_2) \quad (9)$$

$$r_{xy} = \cos\theta_5 (\cos\theta_2 \cos\theta_3 - \sin\theta_2 \sin\theta_3) + \cos\theta_4 \sin\theta_5 (\cos\theta_2 \sin\theta_3 + \cos\theta_3 \sin\theta_2) \quad (10)$$

$$r_{xz} = -\sin\theta_4 (\cos\theta_2 \sin\theta_3 + \sin\theta_2 \cos\theta_3) \quad (11)$$

$$r_{yx} = \sin\theta_5 (\cos\theta_2 \sin\theta_3 + \sin\theta_2 \cos\theta_3) + \cos\theta_4 \cos\theta_5 (\cos\theta_2 \cos\theta_3 - \sin\theta_2 \sin\theta_3) \quad (12)$$

$$r_{yy} = \cos\theta_5 (\cos\theta_2 \sin\theta_3 + \sin\theta_2 \cos\theta_3) - \cos\theta_4 \sin\theta_5 (\cos\theta_2 \cos\theta_3 - \sin\theta_2 \sin\theta_3) \quad (13)$$

$$r_{yz} = \sin\theta_4 (\cos\theta_2 \cos\theta_3 - \sin\theta_2 \sin\theta_3) \quad (14)$$

$$r_{zx} = \sin\theta_4 \cos\theta_5 \quad (15)$$

$$r_{zy} = -\sin\Theta_4 \sin\Theta_5 \tag{16}$$

$$r_{zz} = -\cos\Theta_4 \tag{17}$$

If we simplify some terms from the rotational matrix (R), equation (18), (19), (20), (21), (22) and (23) were obtained, respectively.

$$r_{yy} = \sin(\Theta_2 + \Theta_3)\cos\Theta_5 - \cos(\Theta_2 + \Theta_3)\cos\Theta_4 \sin\Theta_5 \tag{18}$$

$$r_{yx} = \sin(\Theta_2 + \Theta_3)\sin\Theta_5 + \cos(\Theta_2 + \Theta_3)\cos\Theta_4 \cos\Theta_5 \tag{19}$$

$$r_{xz} = -\sin(\Theta_2 + \Theta_3)\sin\Theta_4 \tag{20}$$

$$r_{xx} = \cos(\Theta_2 + \Theta_3)\sin\Theta_5 - \sin(\Theta_2 + \Theta_3)\cos\Theta_4 \cos\Theta_5 \tag{21}$$

$$r_{xy} = \cos(\Theta_2 + \Theta_3)\cos\Theta_5 + \sin(\Theta_2 + \Theta_3)\cos\Theta_4 \sin\Theta_5 \tag{22}$$

$$r_{yz} = \cos(\Theta_2 + \Theta_3)\sin\Theta_4 \tag{23}$$

With similar manner, the solution for the T matrix (T) that shows the position of the end effector is subdivided to $P_{\_}$, where solutions for P_x , P_y and P_z is obtained at (24), (25) and (26), respectively.

$$P_x = a_5 \sin\Theta_5 (\cos\Theta_2 \cos\Theta_3 - \sin\Theta_2 \sin\Theta_3) - a_5 \cos\Theta_4 (\cos\Theta_2 \sin\Theta_3 + \sin\Theta_2 \cos\Theta_3) - a_2 \sin\Theta_2 - a_3 \cos\Theta_2 \sin\Theta_3 - a_3 \sin\Theta_2 \cos\Theta_3 - a_5 \cos\Theta_4 \cos\Theta_5 (\cos\Theta_2 \sin\Theta_3 + \sin\Theta_2 \cos\Theta_3) \tag{24}$$

$$P_y = a_1 + a_2 \cos\Theta_2 + a_4 \cos\Theta_4 (\cos\Theta_2 \cos\Theta_3 - \sin\Theta_2 \sin\Theta_3) + a_5 \sin\Theta_5 (\cos\Theta_2 \sin\Theta_3 + \sin\Theta_2 \cos\Theta_3) + a_3 \cos\Theta_2 \cos\Theta_3 - a_3 \sin\Theta_2 \sin\Theta_3 + a_5 \cos\Theta_4 \cos\Theta_5 (\cos\Theta_2 \cos\Theta_3 - \sin\Theta_2 \sin\Theta_3) \tag{25}$$

$$P_z = d_1 + a_4 \sin\Theta_4 + a_5 \sin\Theta_4 \cos\Theta_5 \tag{26}$$

3.2. Dynamic Model

Dynamical investigation of the robot manipulator enables us to bring about the velocity, acceleration, forces and torques. The output parameters can be calculated with several modeling method [17]. These methods include Recursive Lagrange (R-L), Newton-Euler (N-E), generalized D'Alambert (G-D) and Lagrange-Euler (L-E) methods

Euler-Lagrange model is adopted for the calculation of dynamics. The Euler-Lagrange method makes use of the energy difference. Equation (27) shows the Lagrange energy that is the difference of the total kinetic energy from the total potential energy. Here, K_i *and* E_i obtained from (28) and (29) are the kinetic and potential energy, respectively.

$$L = \sum K_i - \sum E_i \tag{27}$$

$$K_i = \frac{1}{2}\left(m_i v_{ci}^T V_{Ci} + {}^{i}w_i^T \, {}^{Ci}I_i \, {}^{i}w_i\right) \tag{28}$$

$$E_i = -m_i \, {}^{i}g^T \, {}^{0}P_{Ci} + E_{ref} \tag{29}$$

Equation (30) is the Lagrange-Euler equation for calculation of the torques. If the Lagrange-Euler transformed into vector representation, (31) and (32) are derived for application torques and forces, respectively [18].

$$\tau = \frac{d}{dt}\left(\frac{dL}{d\dot{\theta}}\right) - \frac{dL}{d\theta} \tag{30}$$

$$\tau_i = D(\theta)\ddot{\theta} + C\left(\theta,\dot{\theta}\right) + G(\theta) \tag{31}$$

$$F_i = D(x)\ddot{x} + C(x,\dot{x}) + G(x) \tag{32}$$

The vector of D, C and G represents mass matrix, corilois matrix and weight vectors, respectively. The equation (32) was used to obtain the torques of the revolute joints ($\theta_2 - \theta_5$) and Equation (32) was used for the prismatic joint. Table 2 presents the parameters used in calculations. The results for torques and force were obtained with iteration of the parameters.

Table 2. The parameters used for each link

Mass (kg)	**Length (m)**	I_{xx} $(kg \cdot m^{-2})$	I_{zz} $(kg \cdot m^{-2})$
1	0.1	0.00333	0.00333

4. Results and Discussion

The results obtained from the kinematic model are presented in this section. Figure 3 shows the position of the first prismatic axis from the reference axis. According to the figure, only Z axis (the prismatic direction) was acted, and this action was linear.

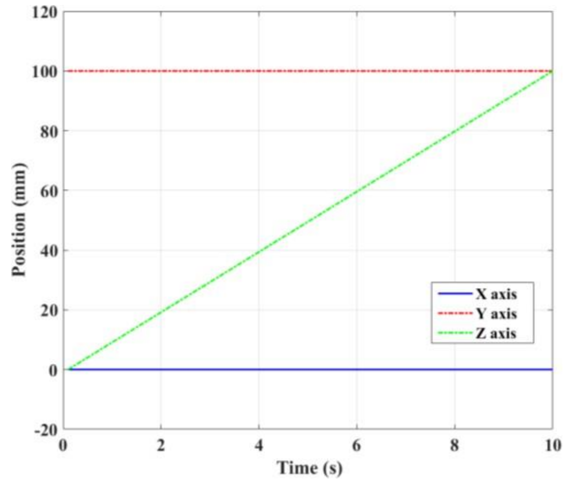

Figure 3. Position of axes for the first prismatic joint.

Figure 4 shows the positions of the revolute axes within joint sequence. According to the figure,

Figure 5 (a), (b), (c) and (d) shows the positions of the A2, A3, A4 and A5 (End-effector) revolute joints mobilized by θ_2, θ_3, $\theta_4, and\ \theta_5$ angles. The Y axes for each revolute joint that adjust the height of the robot manipulator performed an upward and downward movement. The width of this curve increased as the back-to-back connection of the joints increased.

X axes mobilized by joints from θ_2, to θ_5 joints performed just slightly linear decrease. Back- to-back connection of the joints increased the tangential curvature at the start and end of the curves for the X axes. Similarly, the movement range was also increased because of the link length that was affected by the back-to-back linkage.

Figure 5 shows application force in terms of action time. The values of the application force is symbolic. Due to the very low mass and length of the links, application force was calculated between -0.045 and 0.045 N force range. 0.1 m movement range with 10 seconds was the other influence. The application force achieved the maximum point at the time of 2.7 s, afterwards, decreased to zero at 5 s. Then, application of the force reversed to retard the mass for overcoming the force produced by moment of inertia. The velocity was maintained as constant within 10 s.

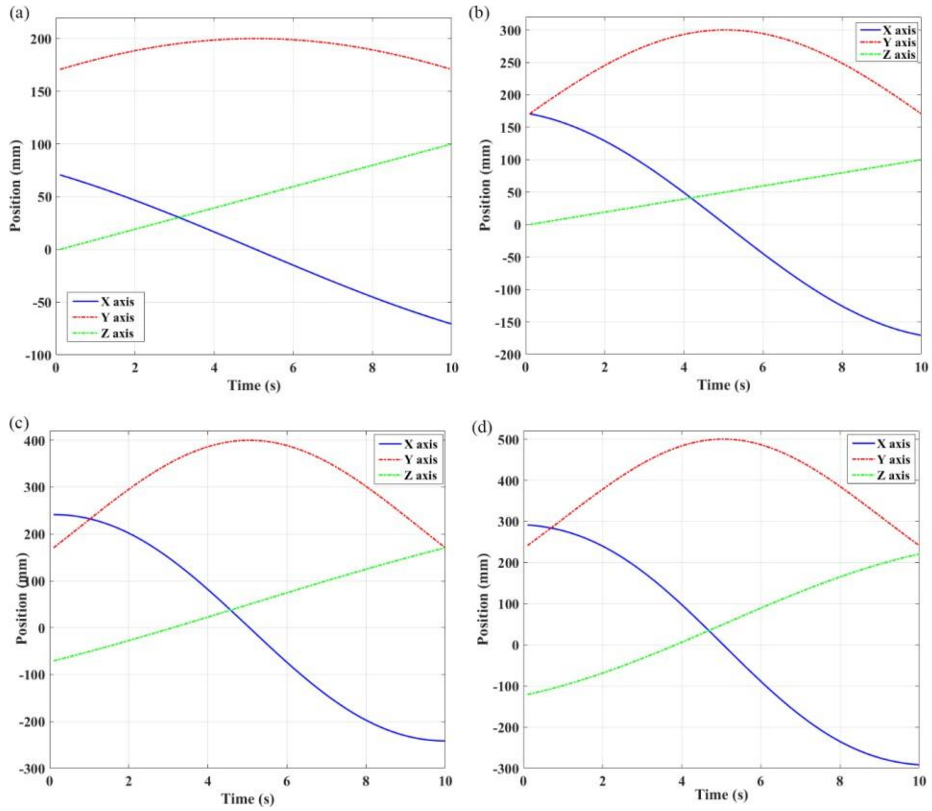

Figure 4. Position of the axes for **(a)** A2 arm induced by θ_2 **(b)** A3 arm induced by θ_3 **(c)** A4 arm induced by θ_4 **(d)** A5 arm (End-effector) induced by θ_5

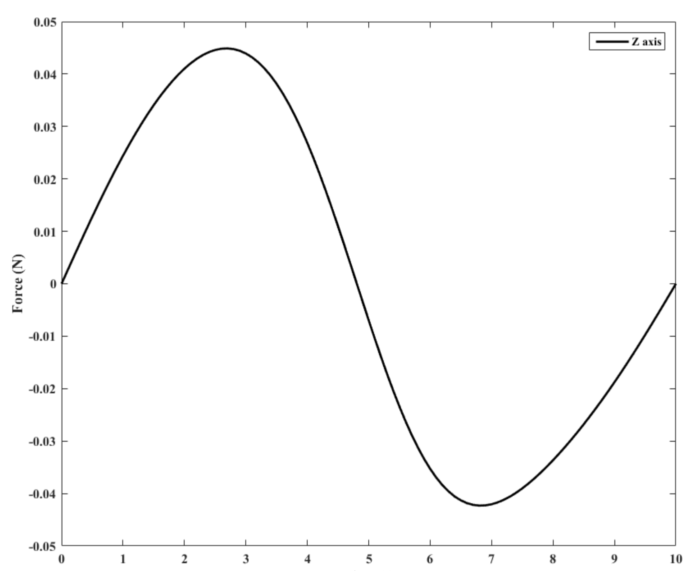

Figure 5. Application force of the first prismatic joint

Figure 6 illustrates the torque produced to maintain velocity of the revolute joints. The torque range was decreased from $\theta_2$to θ_5. The maximum torque for the joints applied by A2 joint, namely, θ_2 as approximately -5 Nm. The minimum torque range belongs to A5 joint with θ_5 since it has only one linkage to drive. The joint of θ_4 has the second minimum torque range because it carries only the A5 arm.

Conclusions

A welder robot manipulator that works with torch application was designed. Kinematic and dynamic calculations were executed. Denavit-Hartenberg method was used for kinematic approach as well as Lagrange-Euler method for dynamics. According to results, the following conclusions can be drawn.

1- The range for the positions of the axes for each manipulator elements were increased as quantity of the back-to-back linkage is increased.

2- The maximum torque was obtained at the A2 link because it carries the whole revolute joints.

3- The moment of inertia and mass of the elements played an important role in determining forces and torques.

4- The range for torques and forces were also affected by the time for experiment.

5- Tangentiality for the curves of X axes was increased due to incremental sum of the axes that have relative tangentiality to neighbor linkages.

References

[1] Valentina DP, Valentina DS, Salvatore M, Stefano R. Smart operators: How Industry 4.0 is affecting the worker's performance in manufacturing contexts. Procedia Comput Sci 2021;180:958–67. https://doi.org/https://doi.org/10.1016/j.procs.2021.01.347.

[2] Meindl B, Ayala NF, Mendonça J, Frank AG. The four smarts of Industry 4.0: Evolution of ten years of research and future perspectives. Technol Forecast Soc Change 2021;168:120784. https://doi.org/https://doi.org/10.1016/j.techfore.2021.120784.

[3] Javaid M, Haleem A, Singh RP, Suman R. Substantial capabilities of robotics in enhancing industry 4.0 implementation. Cogn Robot 2021;1:58–75. https://doi.org/https://doi.org/10.1016/j.cogr.2021.06.001.

[4] O'Shea N, Fenelon MA. Process Instrumentation, Robotics, Wearables and Industry Internet of Things. In: McSweeney PLH, McNamara JP, editors. Encycl. Dairy Sci. (Third

Ed. Third Edit, Oxford: Academic Press; 2022, p. 371–80. https://doi.org/https://doi.org/10.1016/B978-0-12-818766-1.00198-7.

[5] Arden NS, Fisher AC, Tyner K, Yu LX, Lee SL, Kopcha M. Industry 4.0 for pharmaceutical manufacturing: Preparing for the smart factories of the future. Int J Pharm 2021;602:120554. https://doi.org/https://doi.org/10.1016/j.ijpharm.2021.120554.

[6] Morgan J, Halton M, Qiao Y, Breslin JG. Industry 4.0 smart reconfigurable manufacturing machines. J Manuf Syst 2021;59:481–506. https://doi.org/https://doi.org/10.1016/j.jmsy.2021.03.001.

[7] Dekle R. Robots and industrial labor: Evidence from Japan. J Jpn Int Econ 2020;58:101108. https://doi.org/https://doi.org/10.1016/j.jjie.2020.101108.

[8] Fan H, Hu Y, Tang L. Labor costs and the adoption of robots in China. J Econ Behav Organ 2021;186:608–31. https://doi.org/https://doi.org/10.1016/j.jebo.2020.11.024.

[9] Kerruish E. Assembling human empathy towards care robots: The human labor of robot sociality. Emot Sp Soc 2021;41:100840. https://doi.org/https://doi.org/10.1016/j.emospa.2021.100840.

[10] (Maggie) Fu X, Bao Q, Xie H, Fu X. Diffusion of industrial robotics and inclusive growth: Labour market evidence from cross country data. J Bus Res 2021;122:670–84. https://doi.org/https://doi.org/10.1016/j.jbusres.2020.05.051.

[11] Faber M. Robots and reshoring: Evidence from Mexican labor markets. J Int Econ 2020;127:103384. https://doi.org/https://doi.org/10.1016/j.jinteco.2020.103384.

[12] Kreutz-delgado, Kenneth ; Seraji H. Kinematic Analysis of 7-DOF Manipulators. R Inst Technol 2015:469–81.

[13] Lin W, Li B, Yang X, Zhang D. Modelling and control of inverse dynamics for a 5-DOF parallel kinematic polishing machine. Int J Adv Robot Syst 2013;10:1–21. https://doi.org/10.5772/54966.

[14] Li Y, Xu Q. Kinematic analysis of a 3-PRS parallel manipulator. Robot Comput Integr Manuf 2007;23:395–408. https://doi.org/10.1016/j.rcim.2006.04.007.

[15] Uchiyama T, Terada H, Mitsuya H. Continuous path control of a 5-DOF parallel-serial hybrid robot. J Mech Sci Technol 2010;24:47–50. https://doi.org/10.1007/s12206-009-1166-x.

[16] Tale Masouleh M, Gosselin C, Saadatzi MH, Kong X, Taghirad HD. Kinematic analysis of 5-RPUR (3T2R) parallel mechanisms. Meccanica 2011;46:131–46. https://doi.org/10.1007/s11012-010-9393-x.

[17] Dar NGA, Ren HÖ, Kozan R. 5 Serbestlik Dereceli Robot Kolunun Modellenmesi ve Kontrolü. 5 Serbestlik Dereceli Robot Kolunun Model ve Kontrolü 2000;17:155–60. https://doi.org/10.16984/saufbed.22465.

[18] Craig JJ. Introduction to Robotics: Mechanics and Control. Pearson- Pretence Hall; 2005.